

# **Supplemental Information**

for

## **Monthly Sea-Surface Temperature, Sea Ice, and Sea-Level Pressure over 1850–2023 from Coupled Data Assimilation**

Vincent T. Cooper<sup>a</sup>, Gregory J. Hakim<sup>a</sup>, Kyle C. Armour<sup>a,b</sup>

<sup>a</sup>Department of Atmospheric and Climate Science, University of Washington, Seattle, WA

<sup>b</sup>School of Oceanography, University of Washington, Seattle, WA

Corresponding Author:

Vincent T. Cooper ([vcooper@uw.edu](mailto:vcooper@uw.edu))

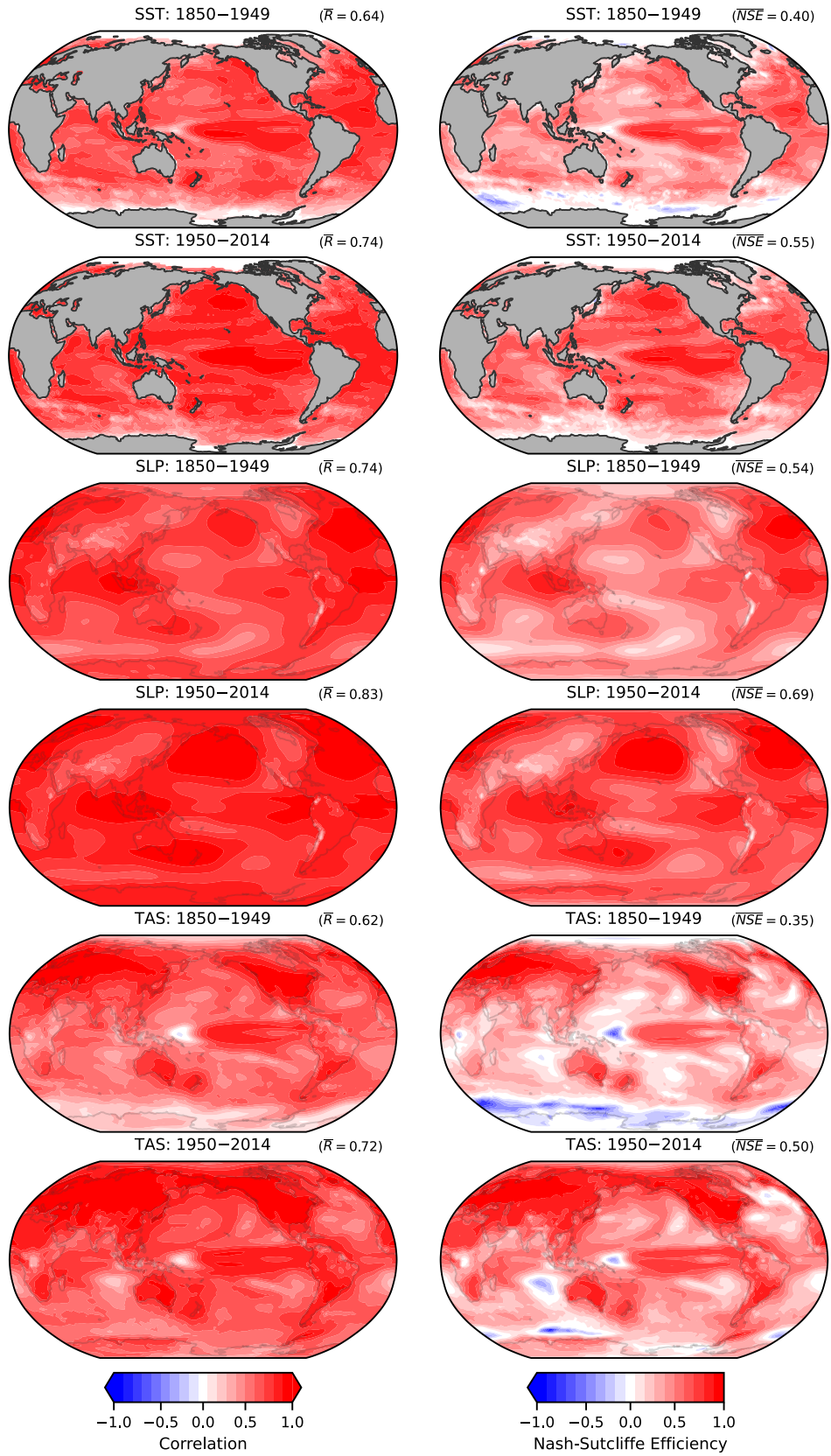


**Figure S1. Pseudo-reconstruction of MPI-ESM1-2-HR: correlation and Nash-Sutcliffe efficiency (NSE) for SST, SLP, and T.** (Left) Local correlation ( $R$ ) of ensemble-mean reconstruction with the target monthly values from MPI-ESM1-2-HR, separately for 1850–1949 and 1950–2014; global mean of local  $R$  is shown in upper right. (Right) Same as left column but showing the local NSE, with the global mean of the local NSE shown in upper right.

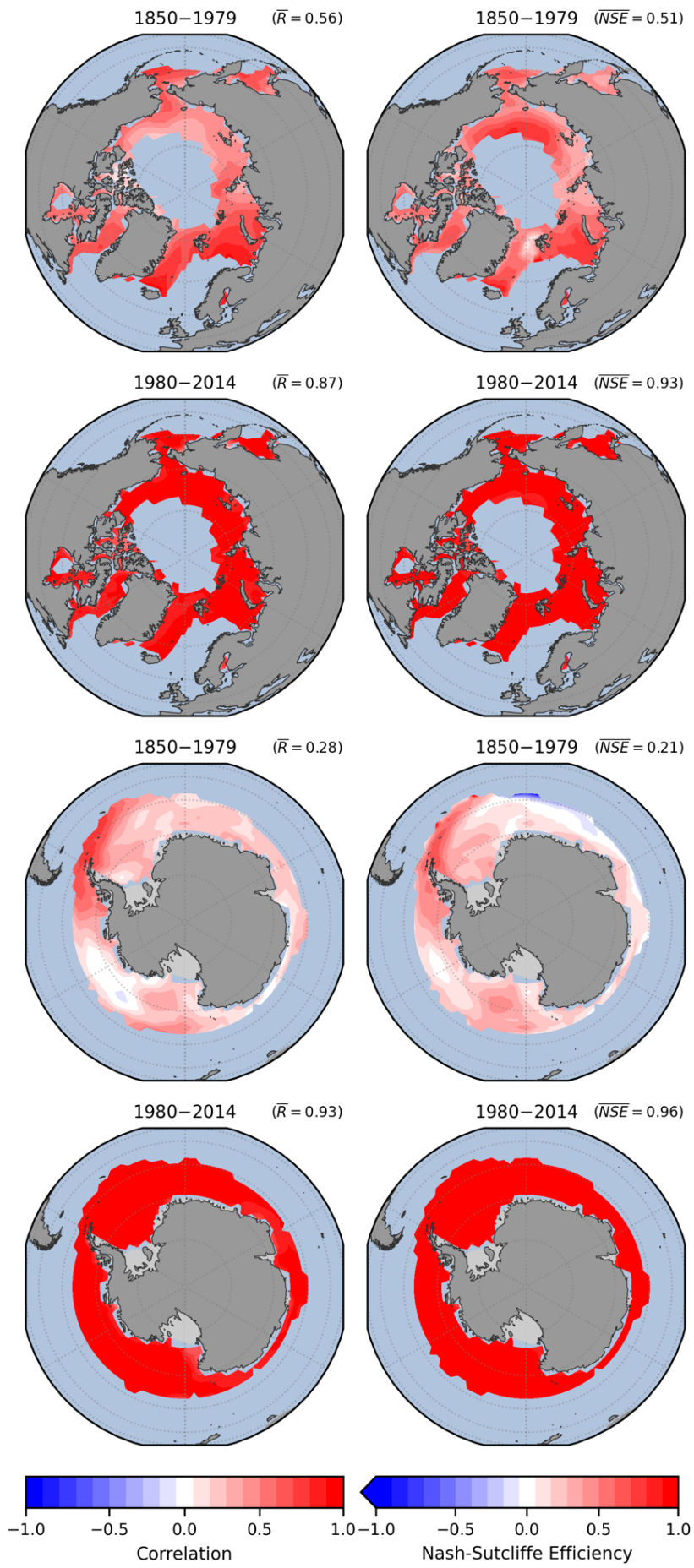


**Figure S2. Pseudo-reconstruction of MPI-ESM1-2-HR: correlation ( $R$ ) and Nash-Sutcliffe efficiency for sea-ice concentration (SIC).** (Left column) Local correlation of ensemble mean from the reconstruction with the true annual values from MPI-ESM1-2-HR's historical simulation, separately for 1850–1979 and 1980–2014, and the global-mean of local correlations is shown in upper right. (Right column) Same as left column but showing the Nash-Sutcliffe Efficiency ( $NSE$ ), with the global mean of the local  $NSE$  shown in upper right.

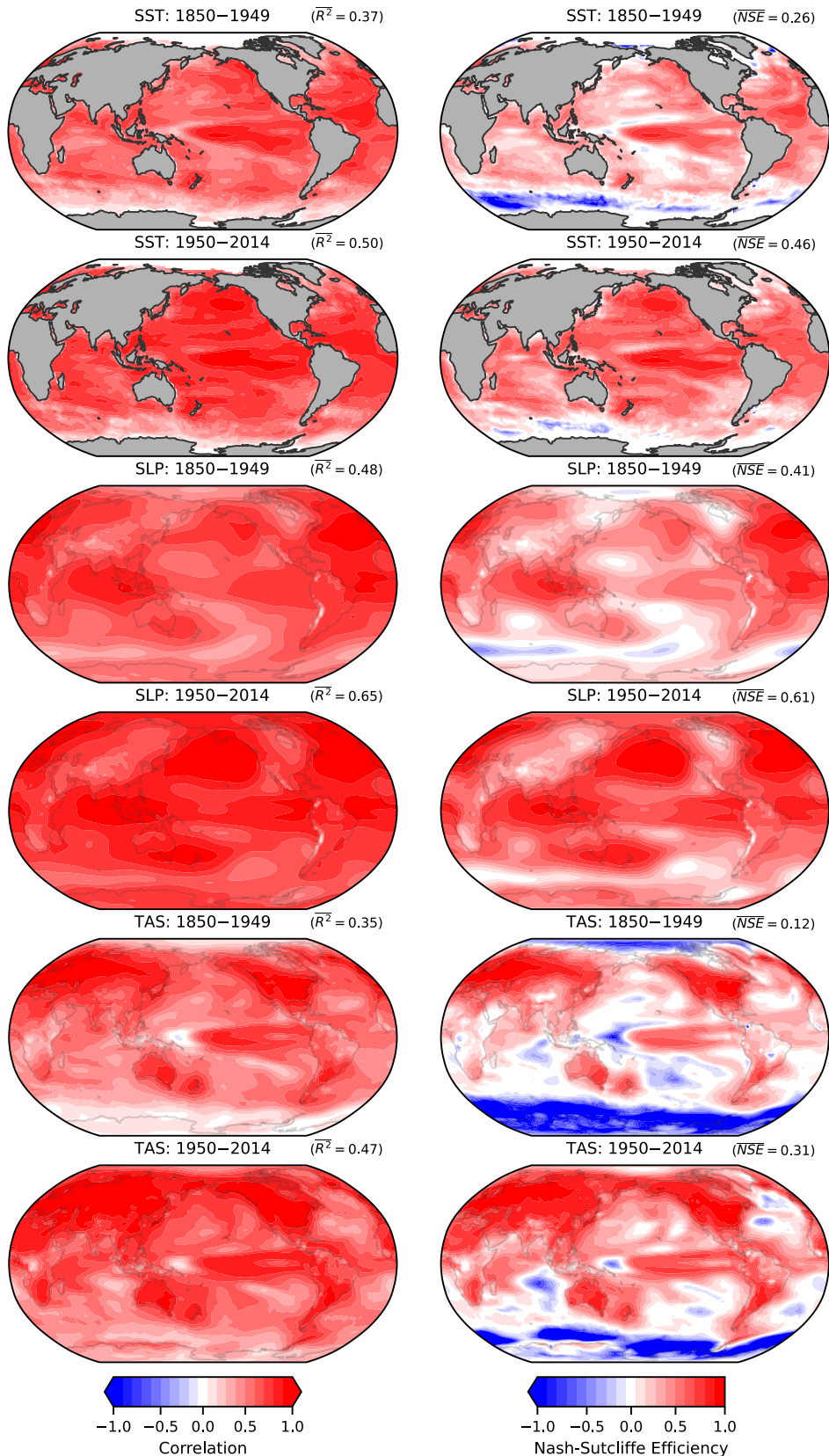


**Figure S3. Pseudo-reconstruction of MPI-ESM1-2-HR, using only a single model prior.** Same as Figure S1, but using only the LIM trained on CESM2 to produce the pseudo-reconstruction (i.e., excluding the other model priors). Compare with Figure S1 to see the benefit of including multiple priors in the reconstruction.

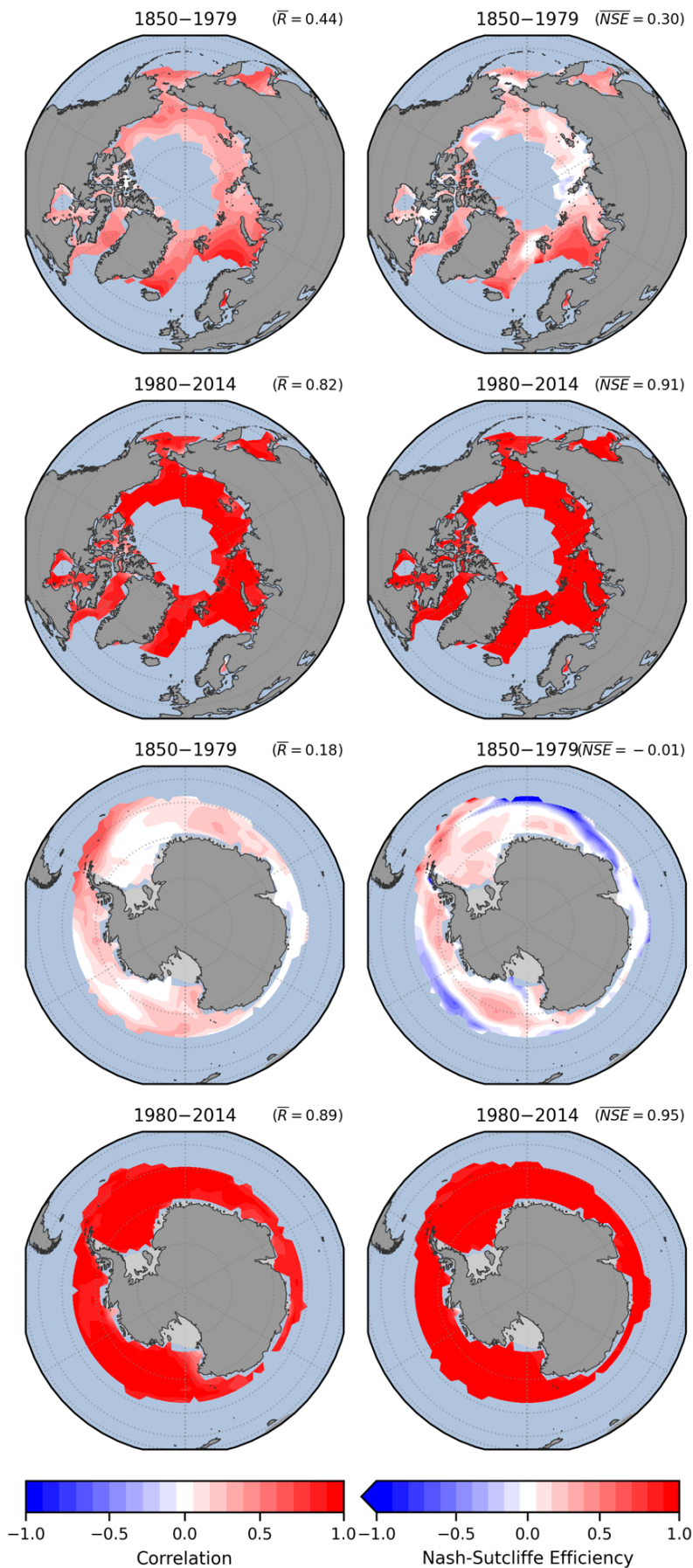


**Figure S4. Pseudo-reconstruction of MPI-ESM1-2-HR, using only a single model prior.**  
Same as Figure S2, but using only the linear inverse model trained on CESM2 to produce the pseudo-reconstruction (i.e., excluding the other model priors). Compare with Figure S2 to see the benefit of including multiple priors in the reconstruction.

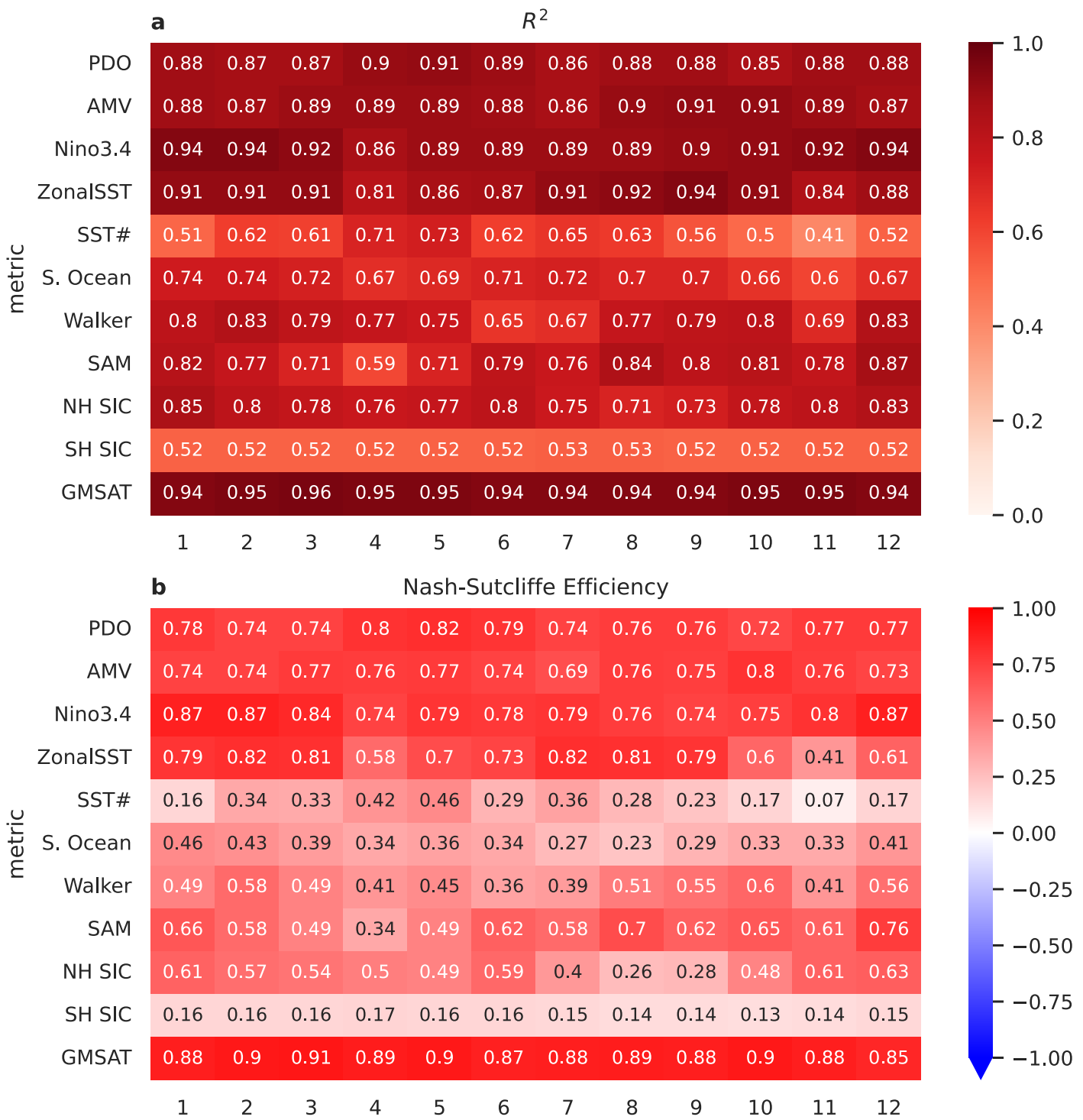


**Figure S5. Validation by pseudo-reconstruction of MPI-ESM1-2-HR: squared Pearson's correlation and Nash-Sutcliffe efficiency by month.** Metrics on the vertical axis correspond to those in Figure 2 but the calculations are based on the monthly resolved data without any low-pass filtering. The horizontal axis represents months January–December. Calculation is over the full pseudo-reconstruction period (1850–2014).

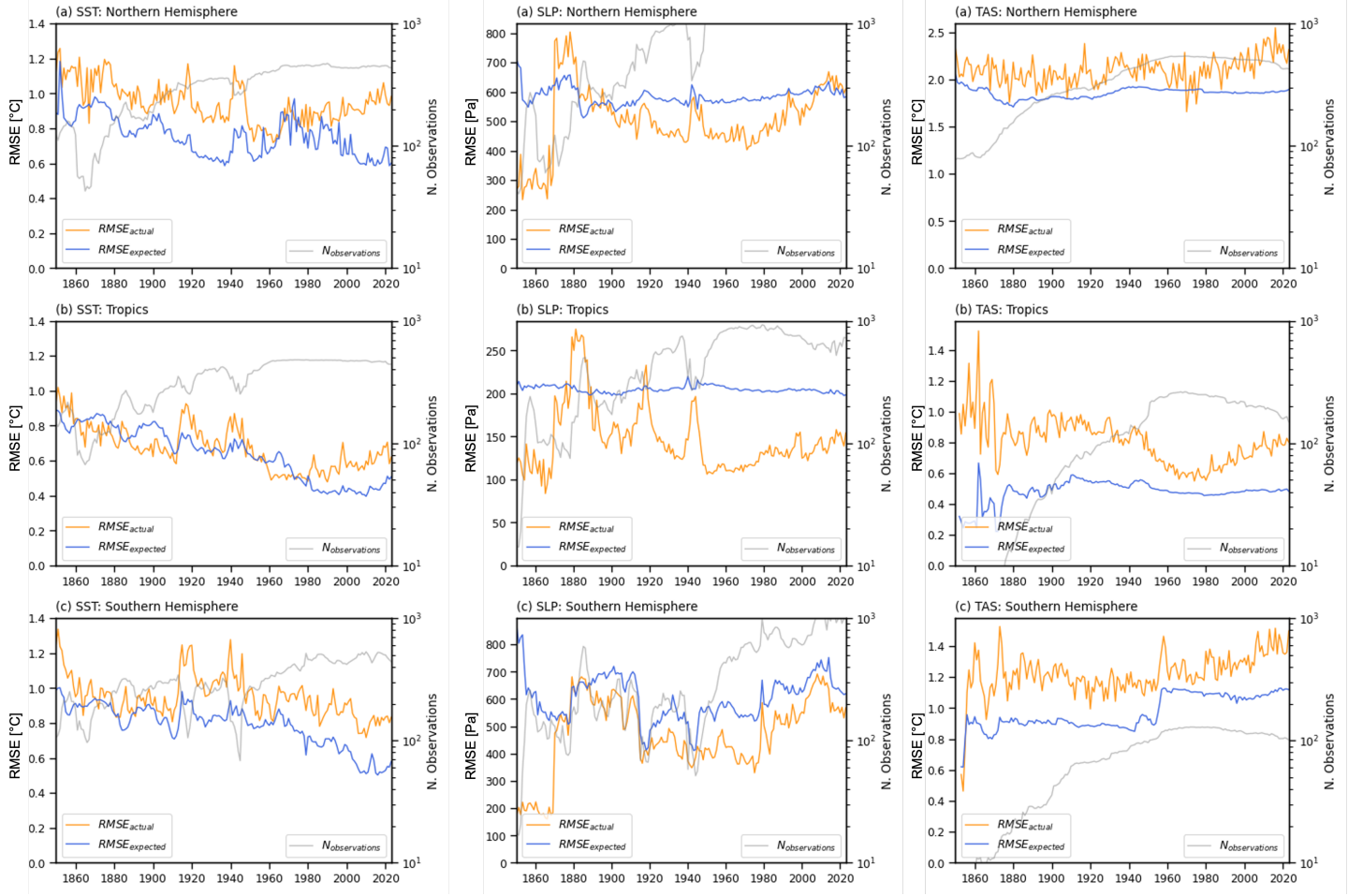


**Figure S6. Desroziers validation statistics.** (Left column) Actual versus expected RMSE averaged for sea-surface temperature over (a) the Northern Hemisphere from  $20^{\circ}$ – $90^{\circ}$ N, (b) the Tropics from  $20^{\circ}$ S– $20^{\circ}$ N, and (c) the Southern Hemisphere from  $20^{\circ}$ – $90^{\circ}$ S. The annual-mean number of observations assimilated per month is shown in gray (right vertical axis). Note that the vertical axes differ between subplots. (Middle column) Same as left column for sea-level pressure. (Right column) Same as left column for near-surface air temperature. All time series show annual means.

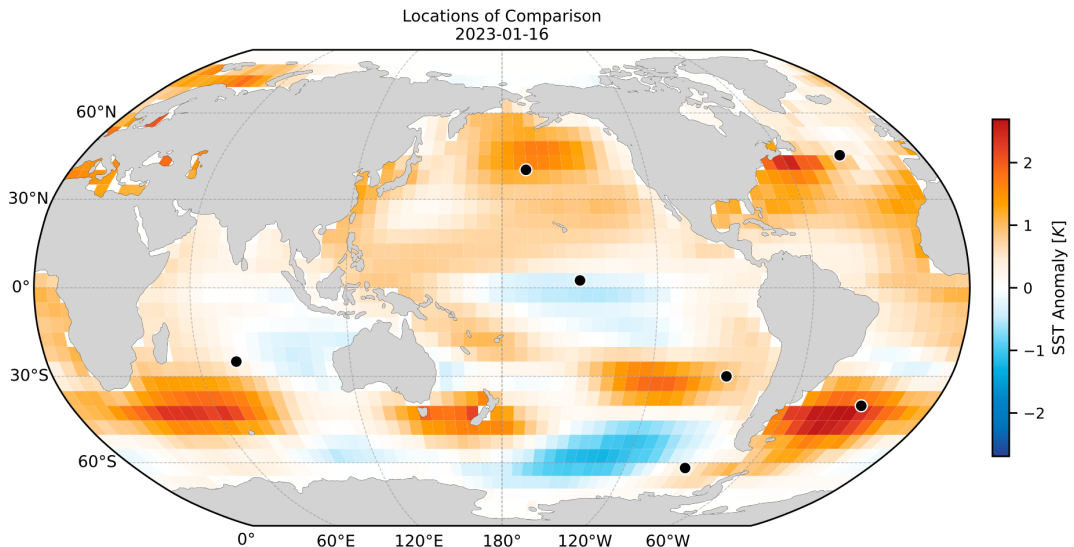


**Figure S7. Select point locations for comparing reconstruction to HadSST4 in following figures.** Black dots indicate the locations shown in Figures S8–S14. The SST plotted shows a single monthly mean, illustrating the January 2023 reconstruction anomaly relative to the 1961–1990 climatology.

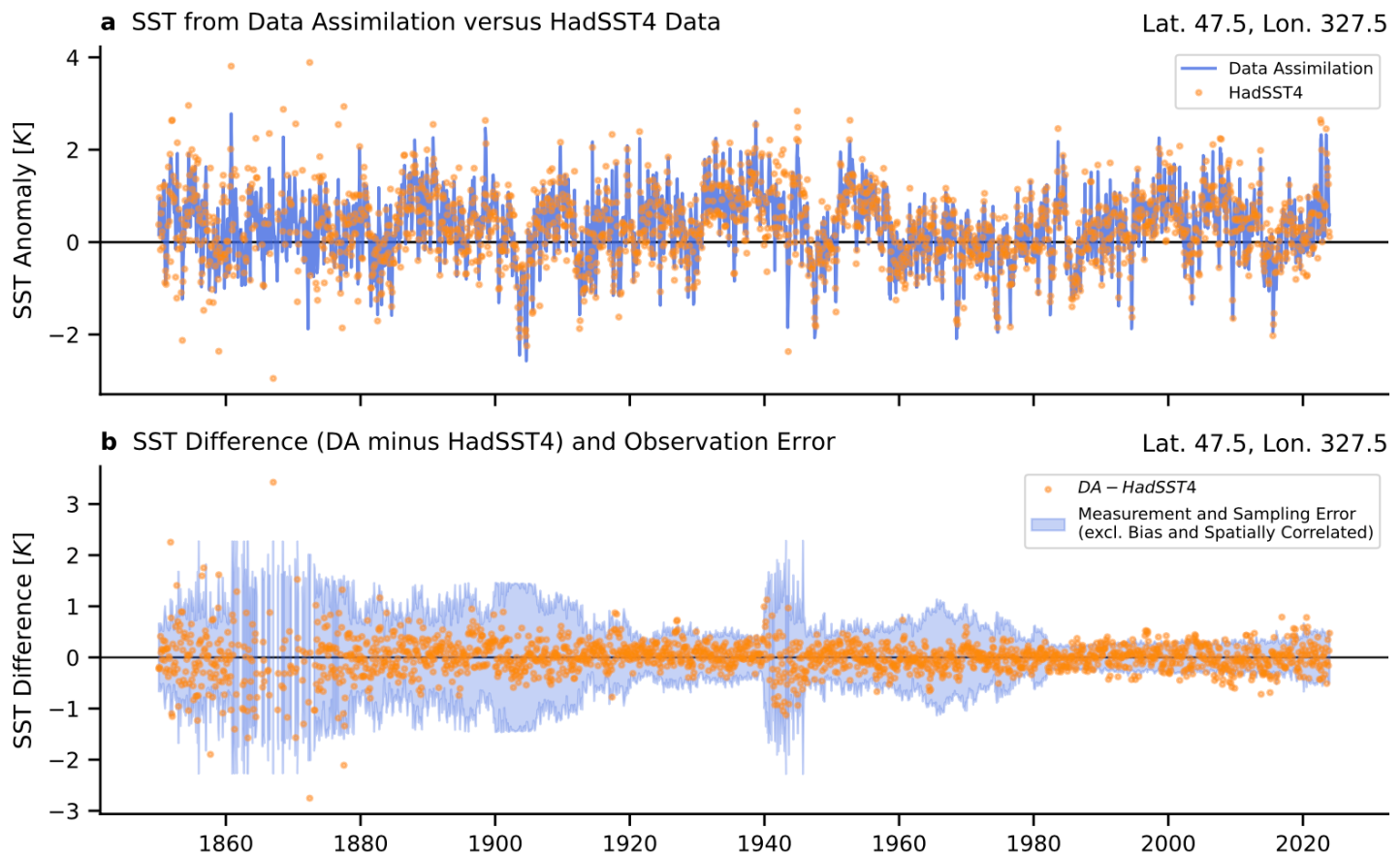


**Figure S8. North Atlantic.** **(a)** Timeseries of SST anomalies in a single gridcell from the data assimilation (DA) ensemble-mean posterior versus the HadSST4 data. **(b)** Analysis residuals, i.e., the SST difference between the DA posterior and HadSST4 data shown, corresponding to panel **a**; Diagonal terms in  $\mathbf{R}$ , i.e., the measurement and sampling error ( $\pm 2\sigma$ ), shown as shading. DA result is regressed to the coarser  $5^\circ$  resolution of HadSST4 for the comparison.

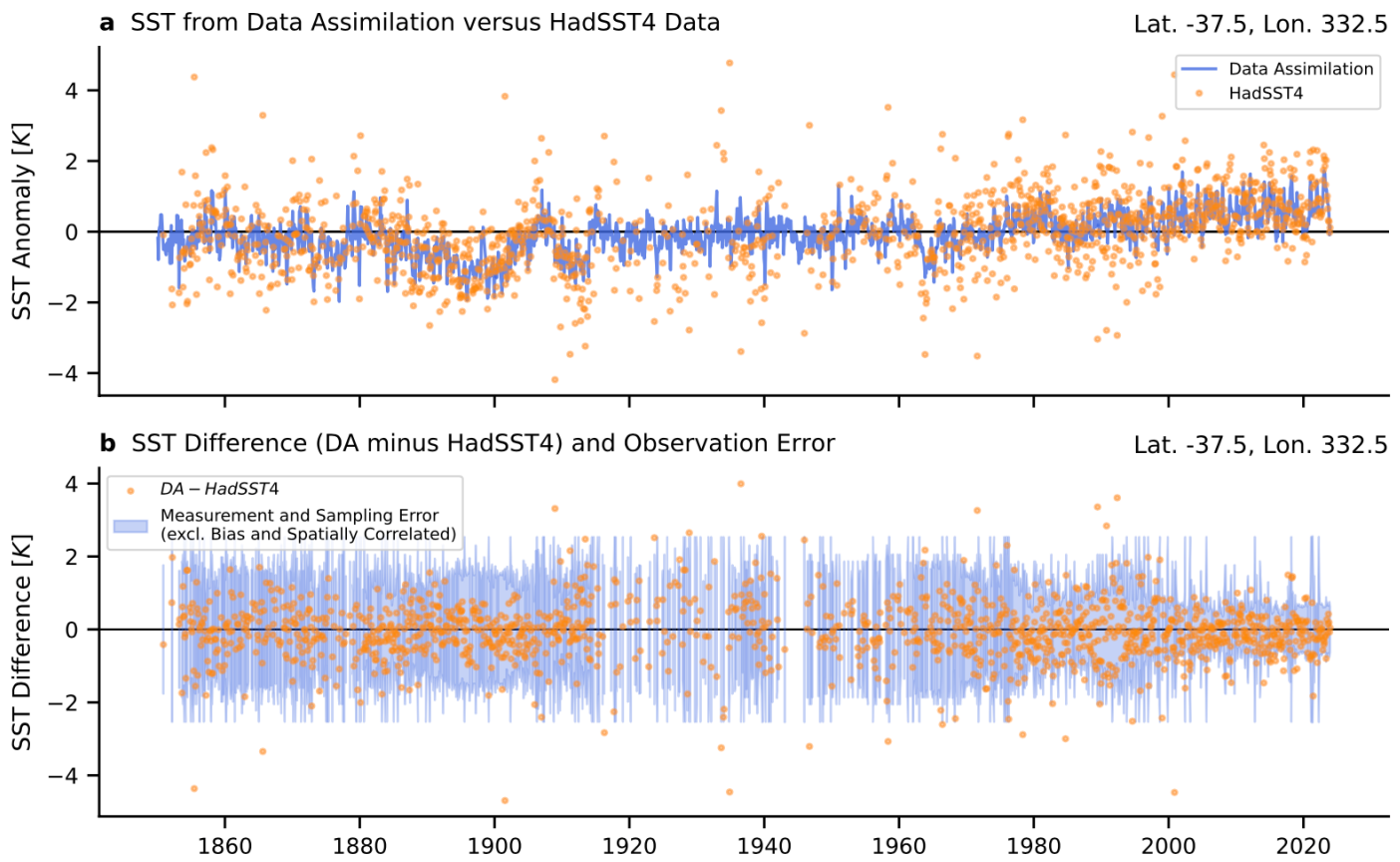


Figure S9. South Atlantic. See caption of Figure S8.

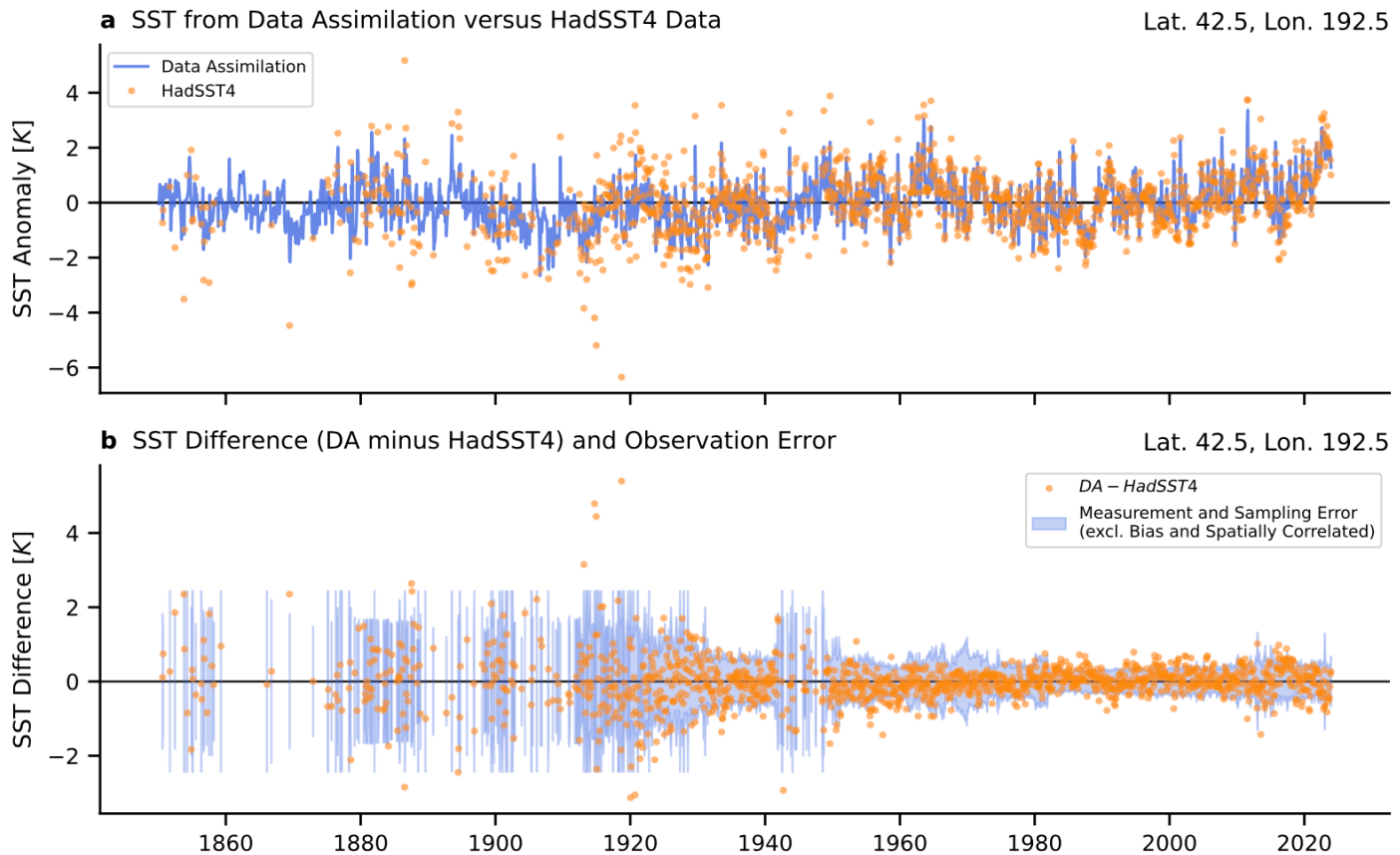


Figure S10. North Pacific. See caption of Figure S8.

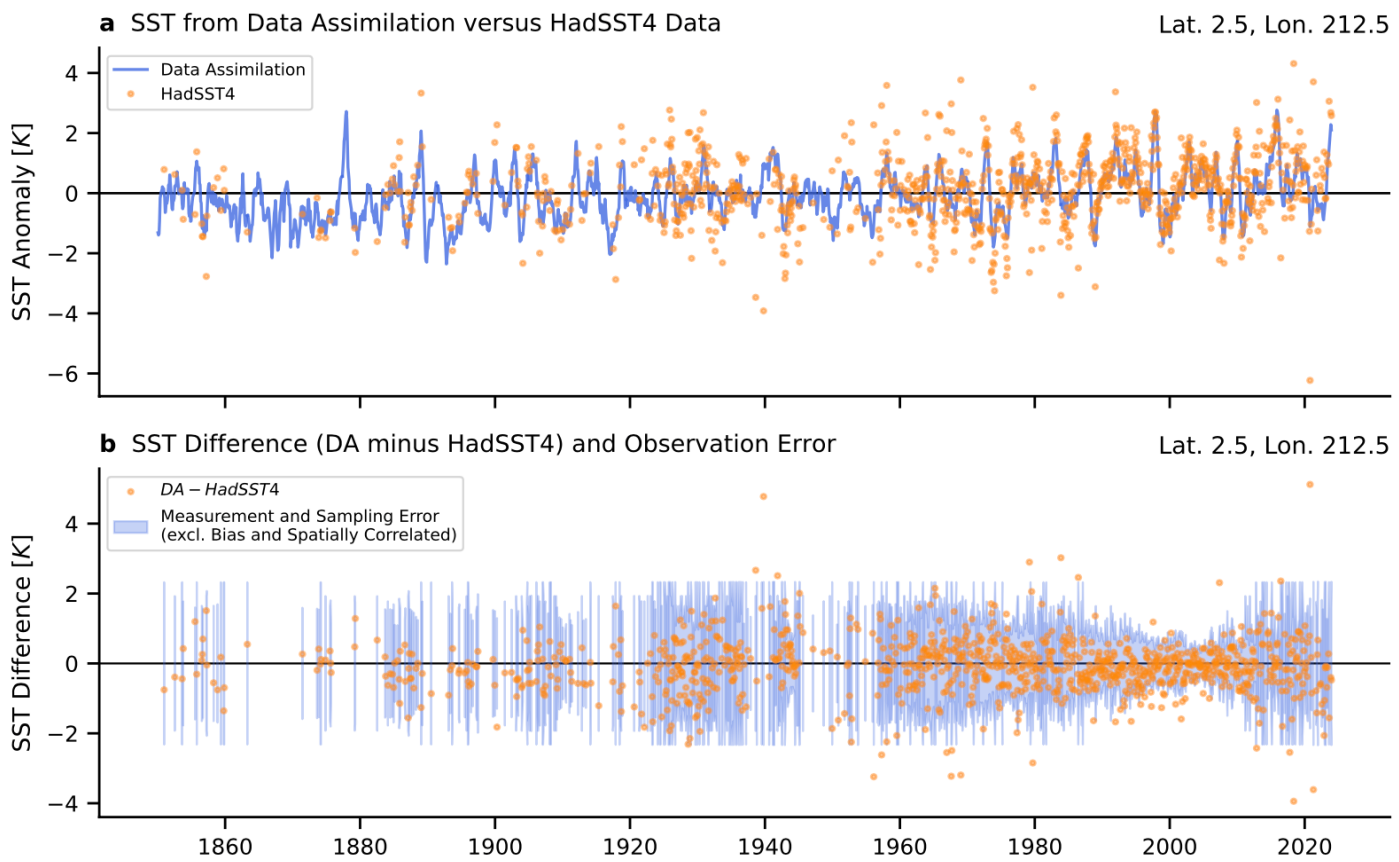


Figure S11. Central Equatorial Pacific. See caption of Figure S8.

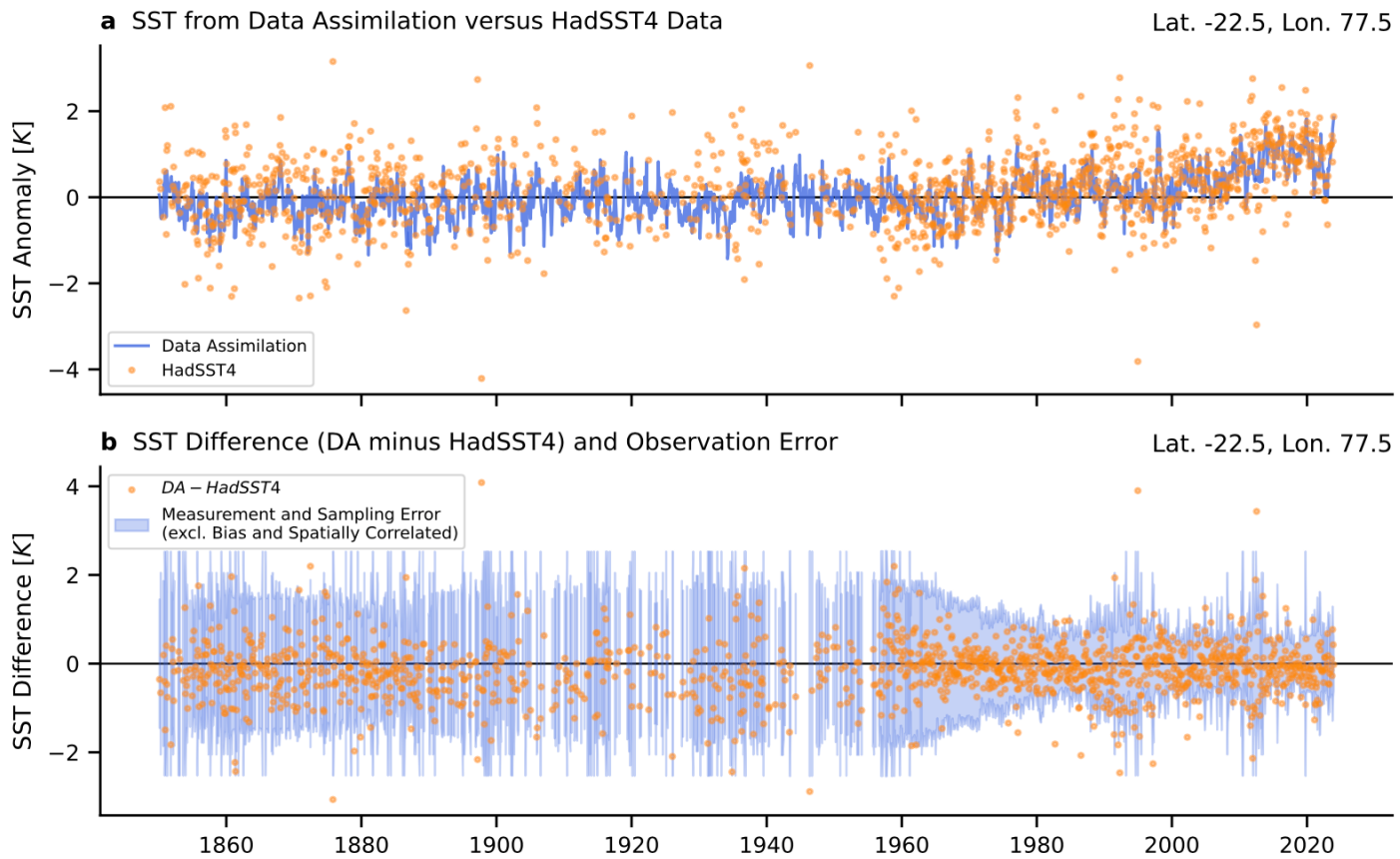


Figure S12. Indian Ocean. See caption of Figure S8.

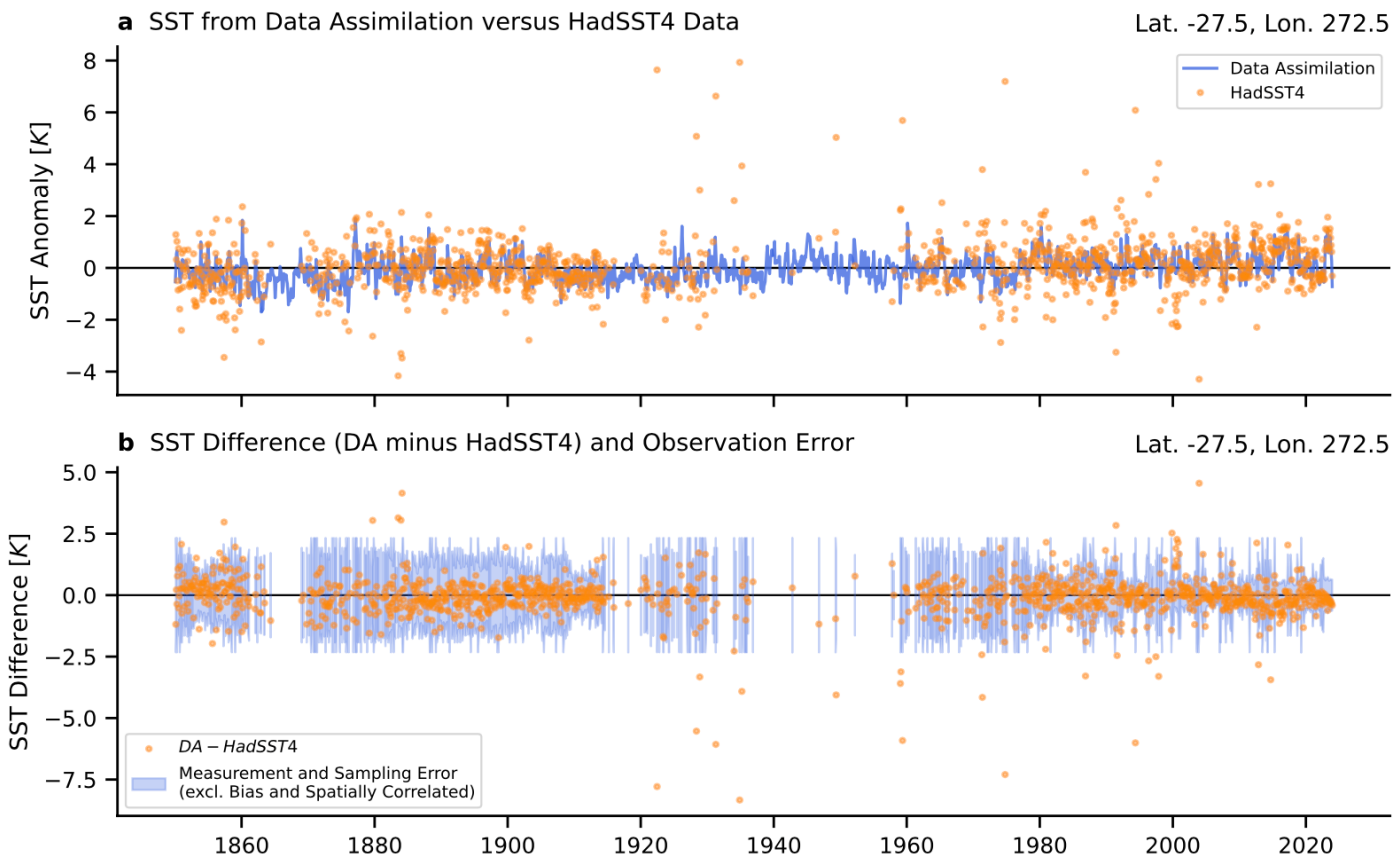


Figure S13. Southeast Pacific. See caption of Figure S8.

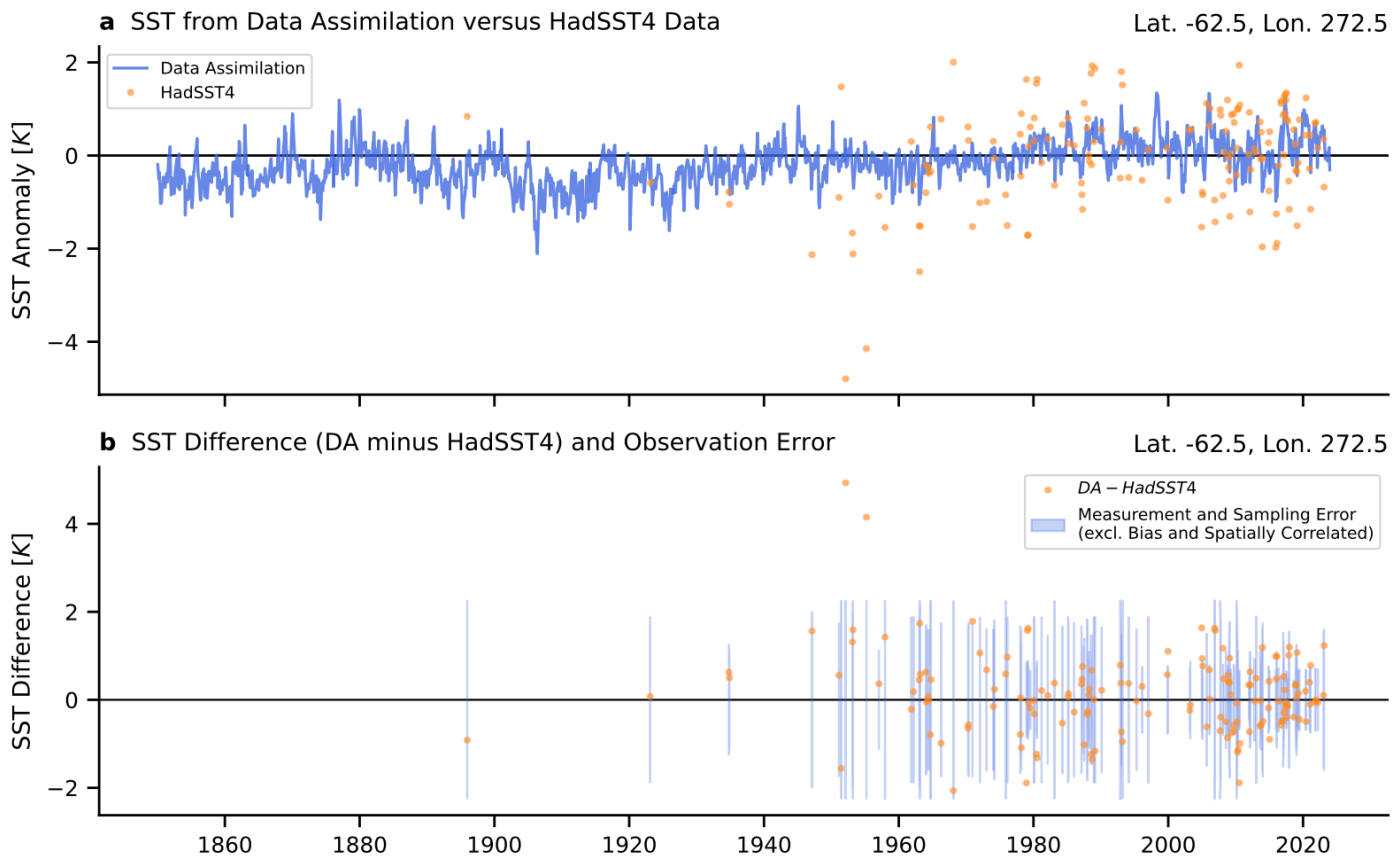
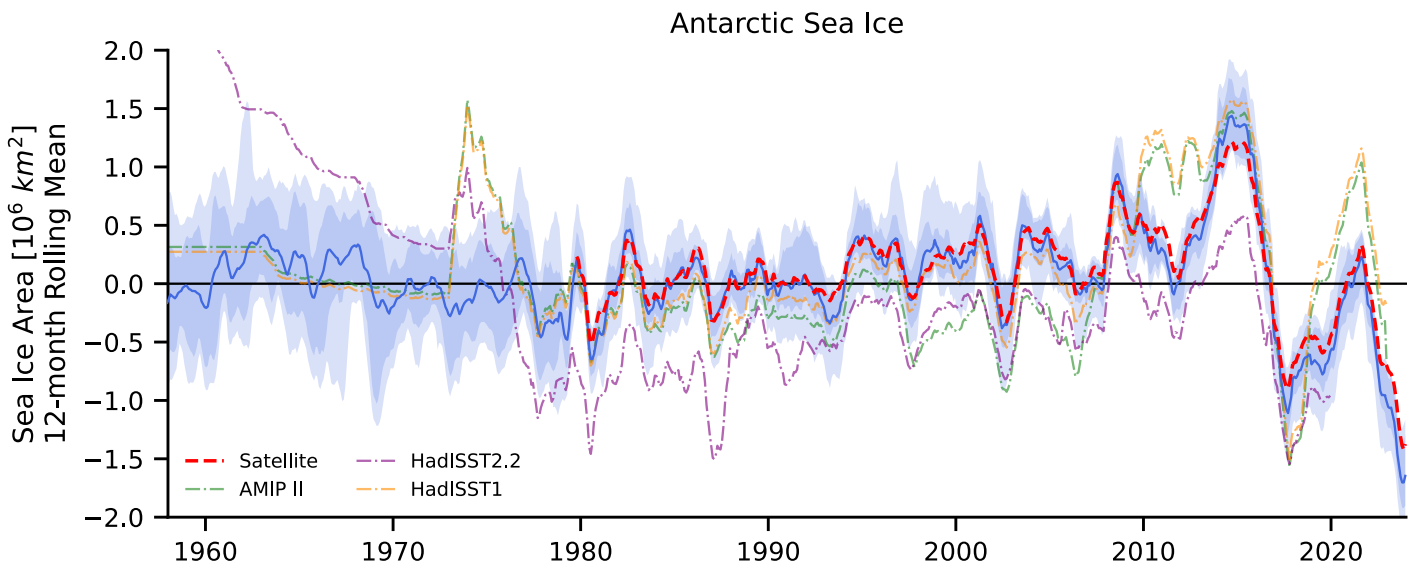
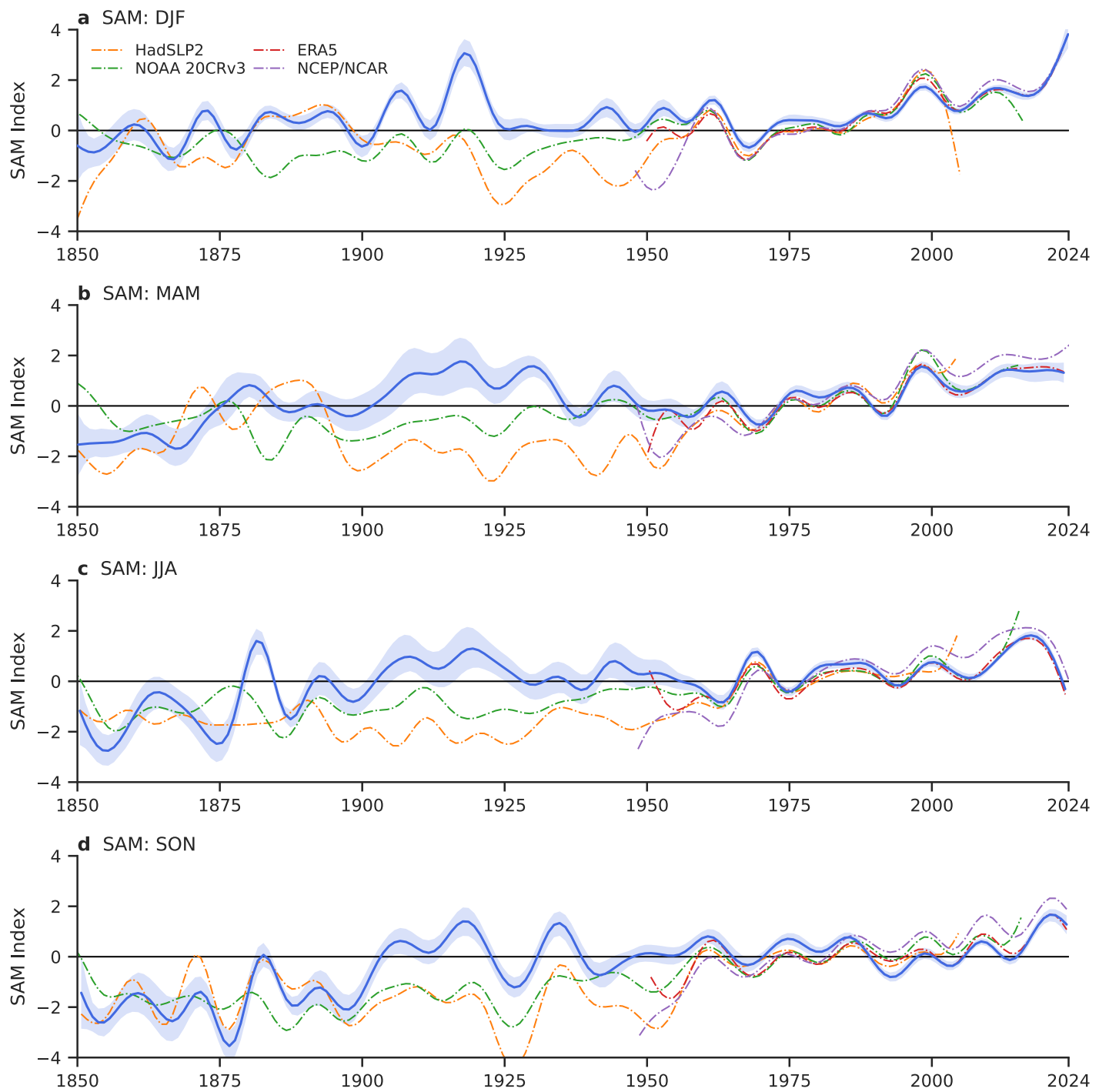


Figure S14. Southern Ocean (SE Pacific Sector). See caption of Figure S8.



**Figure S15. Antarctic sea ice area, 1958–2024.** As shown in Figure 5 but limited to recent decades. Data assimilation results are shown in blue (mean, 66% range, and 90% range). All timeseries are filtered with a 12-month running mean of the monthly means. Anomalies are relative to the 1961–1990 baseline.



**Figure S16. Seasonal values of the Southern Annular Mode (SAM).** As shown in Figure 5 but for separate seasons. Data assimilation results are shown in blue (mean, 66% range). All timeseries are filtered with a 10-year low-pass filter on the monthly means. Anomalies are relative to the 1961–1990 baseline.

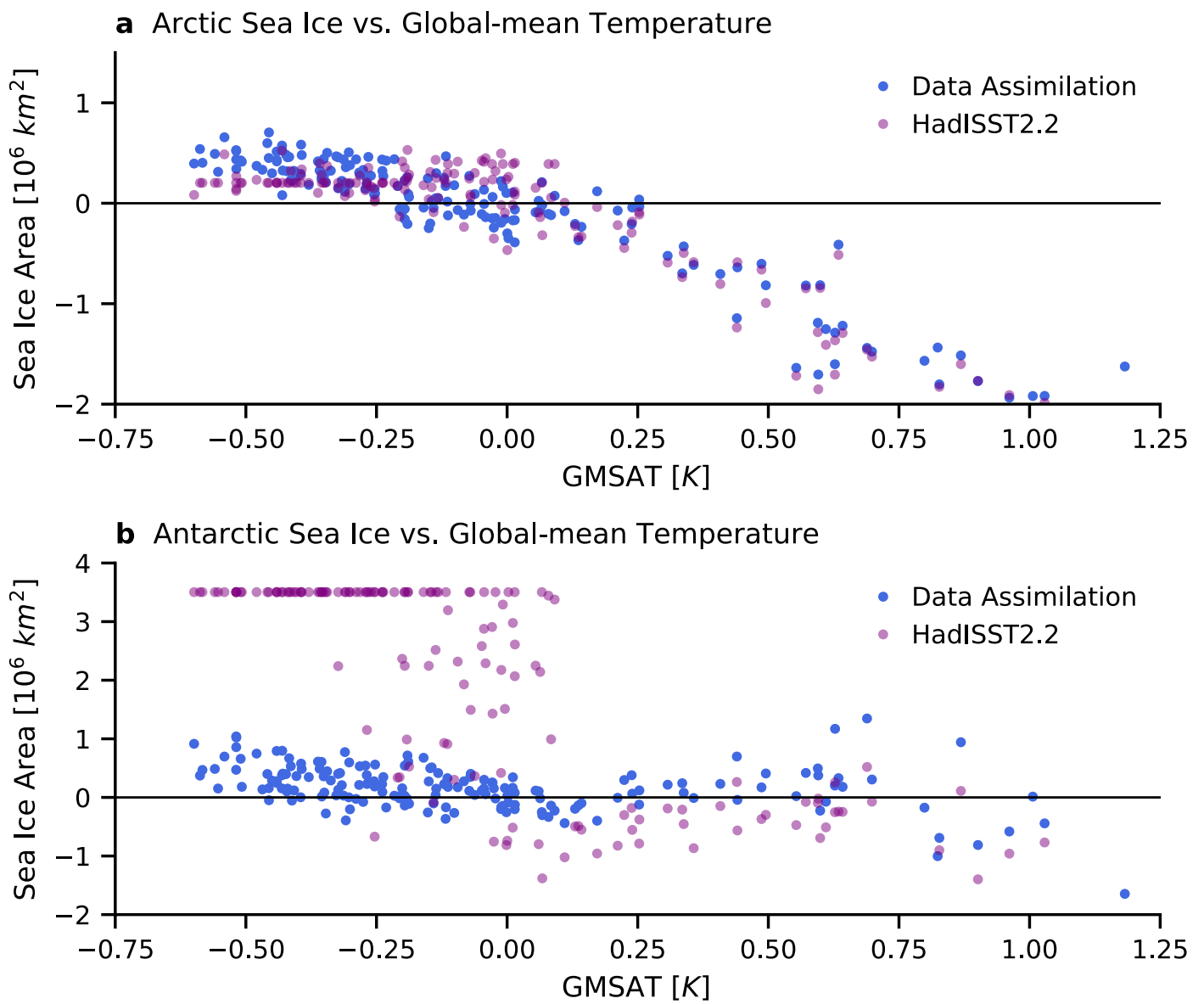


**Figure S17. Sea ice area versus global-mean near-surface air temperature (GMSAT).** Using annual means of the results from data assimilation shown in Figure 5, **(a)** scatter plot of anomalies in total Arctic sea ice area versus anomalies in GMSAT, and **(b)** repeated for the Antarctic.